



# Biogeophysical feedbacks enhance the Arctic terrestrial carbon sink in regional Earth system dynamics

W. Zhang<sup>1</sup>, C. Jansson<sup>2</sup>, P. A. Miller<sup>1</sup>, B. Smith<sup>1</sup>, and P. Samuelsson<sup>2</sup>

<sup>1</sup>Department of Physical Geography and Ecosystem Science, Lund University, 223 62 Lund, Sweden

<sup>2</sup>Rosby Centre, Swedish Meteorological and Hydrological Institute, 601 76, Norrköping, Sweden

Correspondence to: W. Zhang (zhang\_wenxin2005@hotmail.com)

Received: 2 April 2014 – Published in Biogeosciences Discuss.: 12 May 2014

Revised: 25 August 2014 – Accepted: 2 September 2014 – Published: 8 October 2014

**Abstract.** Continued warming of the Arctic will likely accelerate terrestrial carbon (C) cycling by increasing both uptake and release of C. Yet, there are still large uncertainties in modelling Arctic terrestrial ecosystems as a source or sink of C. Most modelling studies assessing or projecting the future fate of C exchange with the atmosphere are based on either stand-alone process-based models or coupled climate–C cycle general circulation models, and often disregard biogeophysical feedbacks of land-surface changes to the atmosphere. To understand how biogeophysical feedbacks might impact on both climate and the C budget in Arctic terrestrial ecosystems, we apply the regional Earth system model RCA-GUESS over the CORDEX-Arctic domain. The model is forced with lateral boundary conditions from an EC-Earth CMIP5 climate projection under the representative concentration pathway (RCP) 8.5 scenario. We perform two simulations, with or without interactive vegetation dynamics respectively, to assess the impacts of biogeophysical feedbacks. Both simulations indicate that Arctic terrestrial ecosystems will continue to sequester C with an increased uptake rate until the 2060–2070s, after which the C budget will return to a weak C sink as increased soil respiration and biomass burning outpaces increased net primary productivity. The additional C sinks arising from biogeophysical feedbacks are approximately 8.5 Gt C, accounting for 22 % of the total C sinks, of which 83.5 % are located in areas of extant Arctic tundra. Two opposing feedback mechanisms, mediated by albedo and evapotranspiration changes respectively, contribute to this response. The albedo feedback dominates in the winter and spring seasons, amplifying the near-surface warming by up to 1.35 °C in spring, while the evapotranspiration feedback dominates in the summer months, and leads

to a cooling of up to 0.81 °C. Such feedbacks stimulate vegetation growth due to an earlier onset of the growing season, leading to compositional changes in woody plants and vegetation redistribution.

## 1 Introduction

Satellite-derived indices, plot-scale surveys and modelling experiments suggest that Arctic terrestrial ecosystems have undergone structural and compositional changes in response to widespread environmental changes in recent decades (Beck and Goetz, 2011; Elmendorf et al., 2012; Miller and Smith, 2012). Vegetation change in turn feeds back to climate via alterations in biogeochemical forcing (e.g. changes in carbon (C) or nutrient cycling that affect greenhouse gases (GHG) emissions) or biogeophysical properties of the land surface such as albedo, roughness length, and partitioning of return energy fluxes from the surface into latent and sensible heat components (Cox et al., 2000; Brovkin et al., 2006). Biogeophysical feedbacks are particularly important for the northern high latitudes (NHLs). Positive albedo feedbacks arising from an expansion and densification of shrublands and forests or from snow-masking by protruding branches and leaves have a large potential to amplify regional climate warming (Chapin et al., 2005; Bonfils et al., 2012). Moreover, biogeophysical feedbacks associated with coupled climate–vegetation dynamics will be linked to biogeochemical feedbacks into the atmosphere through their influence on the terrestrial C and water cycles (Bonan, 2008). Most modelling studies assessing or projecting the state of the C budget for Arctic tundra or the NHLs are based on either stand-alone

process-based models or coupled climate–Carbon cycle general circulation models (GCMs), also known as Earth system models (ESMs) (Sitch, 2008; Qian et al., 2010; McGuire et al., 2012). In general, these studies disregard biogeophysical feedbacks likely to modify initial climate forcing substantially at the local or regional scale under high GHG emission scenarios and consequently affect biogeochemical cycling. In this regard, it is critical to understand the role of biogeophysical feedbacks for both Arctic climate change and terrestrial ecosystems' C balance, especially if their impact on near-surface temperatures is, as some estimates indicate, of a similar order of magnitude as biogeochemical mechanisms (Betts, 2000; Bathiany et al., 2010).

### 1.1 Filling gaps in biogeophysical feedback loops by employing a regional Earth system model

Traditionally, C stores and fluxes simulated by dynamic vegetation models (DVMs) reflect passive responses of terrestrial ecosystems to spatial and temporal variations in climate, since such climate is generated by climate models which often represent vegetation as either a static or an asynchronous dynamic component in the climate system (Quillet et al., 2010). To fill gaps in the biogeophysical feedback loops relies on climate models being tightly coupled with DVMs, which can often trigger cascading impacts to amplify or dampen climate change (Fig. 1). When it comes to Arctic tundra or the NHLs, enhanced solar radiation absorption and near-surface warming are expected to directly stimulate plants' photosynthesis, leading to increased leaf area index (LAI) in the growing season (Piao et al., 2006), and eventually to change vegetation composition and distribution, such as occurs, for example, with a northward invasion of trees and tall shrubs into extant tundra areas (Tape et al., 2006; Miller and Smith, 2012). Ecosystems comprised of taller plants with bigger leaves have higher vegetation roughness, and can accentuate vertical mixing of eddy fluxes, resulting in more efficient transport of momentum, heat and moisture from the canopy to the atmosphere. Accordingly, a negative feedback loop is signified by increased latent heat fluxes, cooling the surface by reducing sensible heating or by weakening atmospheric heating due to a greater abundance of low clouds. On the other hand, invading vegetation or increased LAI may darken the surface, particularly through shading of snow in late winter and spring, and reduce surface albedo, leading to a positive feedback to near-surface temperature. Previous studies of vegetation feedbacks to precipitation have been inconclusive, with indications of positive, negative and minimal feedbacks (Seneviratne et al., 2010; Keuper et al., 2012), but they are likely associated with factors such as wetness of ecosystems, enhanced evapotranspiration and soil moisture, convective characteristics of climate and land-surface heterogeneities.

Recently, ESMs have started to include interactive vegetation dynamics in their land-surface components in order

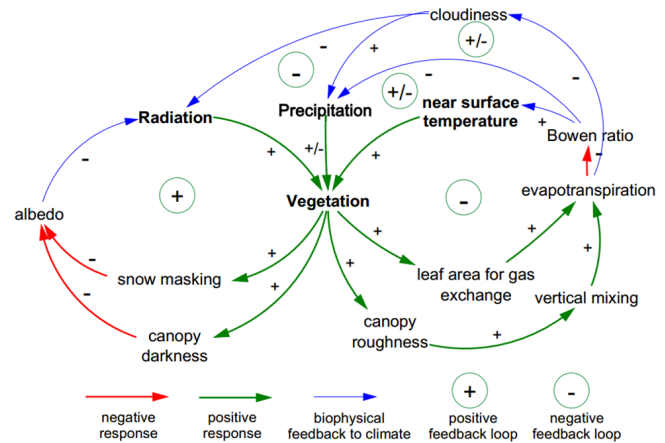


**Figure 1.** Diagram of climate–vegetation interaction feedback loops that comprise positive responses (green), negative responses (red) arising from vegetation change and consequent biogeophysical feedbacks to climate (blue).

to fully address the effects of both biogeochemical and biogeophysical feedbacks arising from land-cover change and land-management practices (e.g. Bathiany et al., 2010; Falloon et al., 2012). However, some processes that occur on a wide range of spatial scales might not be well represented due to their rather coarse resolution. For example, Lorant et al. (2014) pointed out that consistent declines in albedo with increasing tree cover, occurring south of latitudinal tree-line, are poorly represented by ESMs, partly because of their relatively coarse resolution. Regional climate models (RCMs) are complementary tools to GCMs, providing high-resolution simulations of the climate over a limited domain forced by GCM-derived fields on the lateral domain boundaries. By accounting for physiographic features such as mountain chains, lakes and coastlines in a more detailed way, they tend to provide more reliable local or regional details of climate information to end-users and policy-making communities (Rummukainen, 2010). Kueppers et al. (2005) showed that a RCM-based climate projection is more suitable for predictions of potential shifts in species' ranges than GCM-based climate projections in California, since land-surface properties, topography, climatologically distinct ecoregions, and local climate variations with distance from the coast are better resolved in the RCM outputs. To better capture biogeophysical feedbacks to climate resulting from vegetation structural changes, Smith et al. (2011) first coupled the individual-based DVM to a RCM. In a case study over Europe, Wramneby et al. (2010) demonstrated both albedo- and evapotranspiration-mediated feedbacks, and found that biogeophysical feedbacks to future warming were relatively modest compared to the radiative forcing of increased global CO<sub>2</sub> concentrations.

## 1.2 Present studies of terrestrial C balance for Arctic tundra and the NHLs

Arctic tundra and boreal forests have sequestered a considerable amount of C during historic and recent geological times (Oechel et al., 1993; Ruckstuhl et al., 2008). However, the current, recent and future C balance of Arctic terrestrial ecosystems is still under debate due to the large uncertainties associated with the various methodologies used to estimate regional C fluxes or due to the large sensitivities associated with various controlling mechanisms (e.g. gradients of climatic and hydrological variability, disturbances, permafrost vulnerability and nutrient constraints) (Hayes et al., 2012). CO<sub>2</sub> flux measurements indicate that warm winters tend to switch old boreal stands from a sink to a source of C by increasing annual respiration (Valentini et al., 2000; Monson et al., 2006). Similarly, studies using remote sensing approaches have identified a trend of decreasing boreal forest productivity in parts of the Arctic in recent years (Beck and Goetz, 2011). By contrast, results of GCM simulations from the Coupled Carbon Cycle Climate Model Intercomparison Project (C4MIP) indicate that the NHLs will be a C sink of  $0.3 \pm 0.3 \text{ Pg C yr}^{-1}$  by 2100 (Qian et al., 2010). Forest inventory data and long-term ecosystem C studies estimate that boreal forests were a sink for atmospheric CO<sub>2</sub> on the order of  $0.5 \pm 0.08 \text{ Pg C yr}^{-1}$  in both the 1990s and 2000s (Pan et al., 2011). Most of this surplus C was stored in dead wood, litter, and soil C pools in European Russia. More recently, a compilation of flux observations and inversion model estimates for Arctic tundra indicate that large uncertainties in the annual exchange of CO<sub>2</sub> between Arctic tundra and the atmosphere cannot distinguish the Arctic terrestrial C budget from neutral balance (McGuire et al., 2012).

Biogeophysical feedbacks involving plant-mediated changes in albedo, evapotranspiration, surface roughness and energy flux partitioning affect the efficiency of the terrestrial biosphere as a sink for CO<sub>2</sub> from the atmosphere. The ESMs studies generally agree that biogeophysical feedbacks to climate warming are positive for the NHLs and are likely give rise to an amplified warming in the future (Falloon et al., 2012). However, the amplified warming is also likely to have positive and counteracting effects on both vegetation net primary productivity (NPP) and soil heterotrophic respiration (HR). These responses increase uncertainties in determining whether Arctic terrestrial ecosystems will be a sink or source of C under future climate change.

In this study, we highlight the importance of including interactive vegetation dynamics in simulations of the future Arctic climate. To this end, we employ a regional ESM (RCA-GUESS) that couples a regional climate model (RCA4) with an individual-based dynamic vegetation-ecosystem model (LPJ-GUESS) to study the coupled evolution of climate, vegetation and ecosystem C balance across the pan-Arctic. By comparing simulations with and without

interactive vegetation dynamics forced by lateral boundary conditions from a GCM under a strong future warming representative concentration pathway (RCP) 8.5 scenario, we analyse how biogeophysical feedbacks arising from distributional and structural change in arctic tundra and boreal forest may impact the Arctic climate and terrestrial C balance. Specifically, we investigate the following questions:

1. How well does RCA-GUESS simulate Arctic climate, vegetation and C fluxes in the recent period?
2. How do biogeophysical feedbacks affect Arctic climate and terrestrial C balance in a warmer, high-CO<sub>2</sub> future climate?
3. What aspects of vegetation change are particularly associated with changes in terrestrial C balance?

## 2 Methods

### 2.1 RCA-GUESS, a regional Earth system model

RCA-GUESS (Smith et al., 2011) is a regional ESM, in which the Land Surface Scheme (LSS) of the regional climate model RCA4 is coupled with dynamic vegetation and ecosystem biogeochemistry simulated by the individual-based vegetation-ecosystem model LPJ-GUESS.

RCA refers to the Rossby Centre Atmosphere regional climate model that has been modified and updated mostly with respect to the parameterization of physical land-surface processes dealing with physiography and cold climate conditions in mid- and high-latitudes (Samuelsson et al., 2011). The LSS in RCA uses separate tiles for forest and open land. The forest tile is further subdivided into fractions for canopy and forest floor and the proportion of broad-leaved versus needle-leaved (coniferous) forest. The open land tile has separate fractions for vegetation and bare soil. When snow is present, both tiles have a fraction of snow covering the ground. All fractions have their own surface energy balance which are weighted together to provide grid-averaged radiative and turbulent fluxes as surface boundary conditions required by the atmospheric numerical model (Samuelsson et al., 2006).

The Lund-Potsdam-Jena General Ecosystem Simulator (LPJ-GUESS) is an individual-based vegetation-ecosystem model optimized to resolve heterogeneities of vegetation structures and functions at the regional and continental scale (Smith et al., 2001). It shares mechanistic formulations for canopy biophysics, phenology, plant physiology and ecosystem C cycling with the global vegetation model LPJ-DGVM (Sitch et al., 2003) and incorporates improved formulations of ecosystem hydrology (Gerten et al., 2004). However, it differs from the generalized large-area parameterization of vegetation structure and population dynamics used in LPJ-DGVM, adopting instead gap model formalisms based on

explicit representations of growth and competition among cohort-averaged woody plant individuals and a herbaceous understory co-occurring within patches differing in age since last disturbance. Woody plants and herbaceous vegetation are parameterized by plant functional types (PFTs), which are parameter sets governing plant traits with regard to morphology, phenology, shade and drought tolerance, fire resistance and bioclimatic limits. LPJ-GUESS has been successfully applied to model dynamic changes of potential natural vegetation (PNV) across biomes of the world, including Europe (e.g. Hickler et al., 2012), and Arctic and Subarctic regions (e.g. Zhang et al., 2013). The performance and behaviour of the model in simulating ecosystem carbon cycle variations and responses to drivers has been highlighted, for example, by Ahlström et al. (2012a, b), Piao et al. (2013) and Smith et al. (2014).

In RCA-GUESS, the vegetation dynamics affects the LSS of RCA by dynamically adjusting the LAI and the relative cover of needle-leaved and broad-leaved forests in the forest tile and herbaceous vegetation in the open land tile. In this study, the six global PFTs used in LPJ-GUESS consist of boreal needle-leaved evergreen trees (e.g. *Picea obovata*, *Picea abies*), boreal shade-intolerant needle-leaved evergreen trees (e.g. *Pinus sylvestris*), boreal needle-leaved deciduous trees (e.g. *Larix sibirica*), temperate broad-leaved deciduous trees (e.g. *Tilia cordata*), boreal shade-intolerant broad-leaved deciduous trees (e.g. *Betula pubescens*) and C3 grass (e.g. *Gramineae*). The parameter sets for characteristic traits of PFTs are given in Table S1 in the Supplement. The simulated daily LAI and phenology state of the needle-leaved and broad-leaved PFTs in LPJ-GUESS are aggregated to the corresponding forest types in the forest tile of RCA (Eq. 1.1 in Table S2 in the Supplement). The relative cover fractions of forests and herbaceous vegetation within the forest and open land tile are estimated as the foliar projective cover computed from the simulated LAI using Lambert Beer's law (Eq. 1.2–1.4 in Table S2 in the Supplement). The returned LAI alters the surface and aerodynamic resistances which are further used by RCA for the calculation of the sensible and latent heat fluxes (Eq. 1.5–1.9 in Table S2 in the Supplement). The fractional size of the forest tile is allowed to vary only if the simulated maximum growing-season LAI summed across forest PFTs is lower than 1, signifying marginal or stunted woody plant growth. The relative covers for forests and open land affect the weighted averaged albedo for each grid cell (Eq. 2.0 in Table S2). The configuration and behaviour of RCA-GUESS is described in detail by Smith et al. (2011).

## 2.2 Model domain, driving data and simulation protocols

The simulations were applied across the Arctic domain of the Coordinated Regional Climate Downscaling Experiment (CORDEX-Arctic). The domain encompasses  $150 \times 156$  grid points with a uniform resolution of  $0.44 \times 0.44^\circ$  (approx-

mately 50 km) by rotating the pole system over an equatorial domain. The boundary conditions were taken from the CMIP5 (Coupled Model Intercomparison Project phase 5) simulations of the EC-Earth GCM (Hazelegger et al., 2010, 2012) for the RCP8.5 scenario (Moss et al., 2010).

RCA-GUESS was initialized by a spin-up phase to achieve an equilibrium state for vegetation structure and composition, C pool and climate conditions appropriate to the period 1961–1990. Compared to the relatively short spin-up necessary for RCA (only a few months), LPJ-GUESS requires a much longer spin-up composed of two stages. In the first stage, LPJ-GUESS is run in an un-coupled mode, forced by climate variables (precipitation, sunshine, temperature) from the CRU TS3.0 (1991–2006) (Climate Research Unit Time Series) observation-based climate data set (Mitchell and Jones, 2005). The first-stage spin-up encompasses 360 years, repeatedly cycling de-trended CRU climate from the period 1901–1930 and the 1901 atmospheric CO<sub>2</sub> concentration of 296 ppm until 1900, and thereafter observed climate and CO<sub>2</sub> until 1960. After 1960, the simulation continues for a further 30 years but in a coupled mode, with RCA-generated climate fields forcing LPJ-GUESS, while LPJ-GUESS returns vegetation properties to RCA. In the second-stage spin-up, a new 360 year spin-up is performed, using a de-trended version of the climate forcing generated by RCA for the period 1961–1990 in the first stage. This two-stage procedure to spin up the vegetation model aims to produce a smooth transition of the climate forcing from the uncoupled spin-up to the coupled (RCA-forced) phase of the final simulation, avoiding a step change in the forcing that may initiate drift in the soil and vegetation carbon pool sizes, disrupting the baseline for the subsequent coupled phase of the simulation. After the spin-up phase, RCA-GUESS was run in the coupled mode for the period 1961–1990. Two simulations were then performed for the period 1991–2100 in coupled and un-coupled modes respectively (hereafter referred to as the feedback run and the non-feedback run). In the non-feedback run, RCA was forced by daily mean vegetation properties averaged from the LPJ-GUESS outputs for the period 1961–1990.

## 2.3 Evaluation of the climate, vegetation and Arctic tundra C balance simulated for the recent period

Outputs from RCA-GUESS for the period 1961–1990 were compared with available observational data sets, omitting the relaxation zone around the domain boundary. Seasonal mean 2 m temperature and total precipitation (the sum of convective and large-scale precipitation) were obtained from two data sets: the CRU TS3.0 and WILLMOTT 3.02 (Willmott and Matsuura, 1995). To evaluate the simulated vegetation distribution, we compared the model-derived dominant PNV map to the map composed using the International Satellite Land Surface Climatology Project (ISLSCP) II PNV Cover data set and the Kaplan PNV data set (Kaplan et al., 2003)

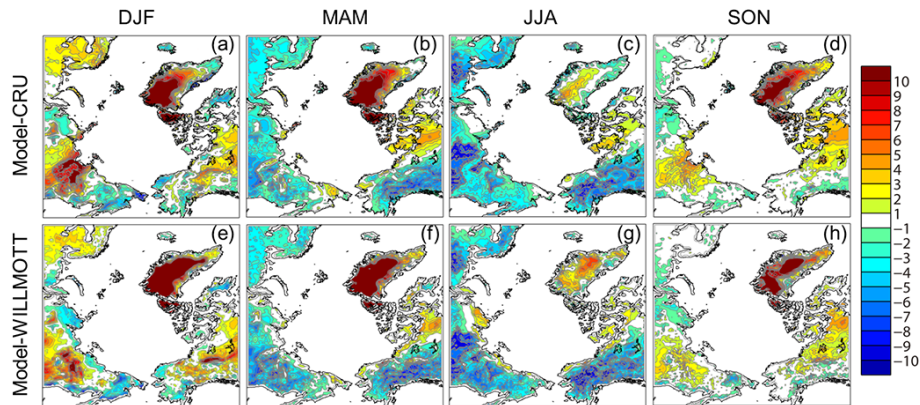


**Figure 2.** The mean seasonal 2m temperature anomalies ( $^{\circ}\text{C}$ ) relative to the CRU and WILLMOTT data sets for the period 1961–1990. (a, e) Winter, December to February (DJF). (b, f) Spring, March to May (MAM). (c, g) Summer, June to August (JJA). (d, h) Autumn, September to November (SON).

based on the same aggregated vegetation classes (see Table S3 in the Supplement). The Kaplan PNV data set supplements the ISLSCP II PNV cover data set with additional details of low and tall shrubs across Arctic tundra. The dominant PNV in the model was derived from the PFTs with the largest LAI in each grid cell. The latitudinal percentage difference for each aggregated vegetation type between the composed map and the simulated map is quantified by the number of grid cells in which the simulation over- or underestimates each vegetation type divided by the total number of grid cells in each latitude band. The simulated NPP flux was evaluated using data from both Arctic tundra and boreal forest data sets: the Ecosystem Model-Data Intercomparison (EMDI) (Olson et al., 2013a), the Biological Productivity of Ecosystems of Northern Eurasia (BAZ) (Denissenko et al., 2013), the Global Primary Production Data Initiative Product, R2 (GPPDI\_1) (Olson et al., 2013b), the Global Primary Production Data Initiative Product, R3 (GPPDI\_2) (Zheng et al., 2013) and the NPP Boreal Forest (BOREAL) (Gower et al., 2012). To evaluate net ecosystem exchange (NEE), the residual difference among the fluxes of NPP, HR and fire disturbance, we compared inter-annual variability of NEE anomalies and mean C budget for an Arctic tundra domain (McGuire et al., 2012; Fig. S1 in the Supplement) to the estimates of process-based models (LPJ-GUESS WHyMe (Wania et al., 2009a, b, 2010; Zhang et al., 2013). Terrestrial Carbon Flux (TCF) model (Kimball et al., 2009), ORCHIDEE (Koven et al., 2009, 2011), Terrestrial Ecosystem Model (TEM; version 6.03) (McGuire et al., 2010; Hayes et al., 2011) and inversion models (Peylin et al., 2013) for the period 1990–2006; for details also see the Appendix in McGuire et al. (2012).

## 2.4 Analysis of impacts of biogeophysical feedbacks to climate, the terrestrial C budget and vegetation change

The impacts of biogeophysical land-atmosphere feedbacks on Arctic climate were quantified as mean seasonal and monthly anomalies of 2 m temperature and total precipitation averaged over the period 2071–2100 in the feedback run relative to the non-feedback run. Anomalies of surface albedo and latent heat flux were calculated to discriminate albedo-from evapotranspiration-mediated feedbacks in their effects on temperature and precipitation.

For the future Arctic terrestrial C budget, we calculated mean C stores and fluxes for Arctic tundra and the CORDEX-Arctic domain respectively, and examined the relative contribution of C sinks from Arctic tundra. We also explored how biogeophysical feedbacks affect C exchange by evaluating the magnitude and year of the peak C-uptake rate for both Arctic tundra and boreal forests.

Climate-induced vegetation shifts were analysed using the percentage of change for a normalized phenology index and a normalized physiognomy index (Wrannby et al., 2010; see Eqs. (2.1)–(2.2) in Table S2 in the Supplement) based on LAI changes of the simulated PFTs averaged over the period 2071–2100 relative to 1961–1990. Biogeophysical feedback-induced vegetation shifts were characterized as the percentage of change for the aforementioned indices for the period 2071–2100 based on the feedback-run relative to the non-feedback run.

## 3 Results

### 3.1 The recent Arctic climate, vegetation and C flux

The simulated mean seasonal climate for 1961–1990 shows a cold bias on the order of  $2^{\circ}\text{C}$  compared to observations

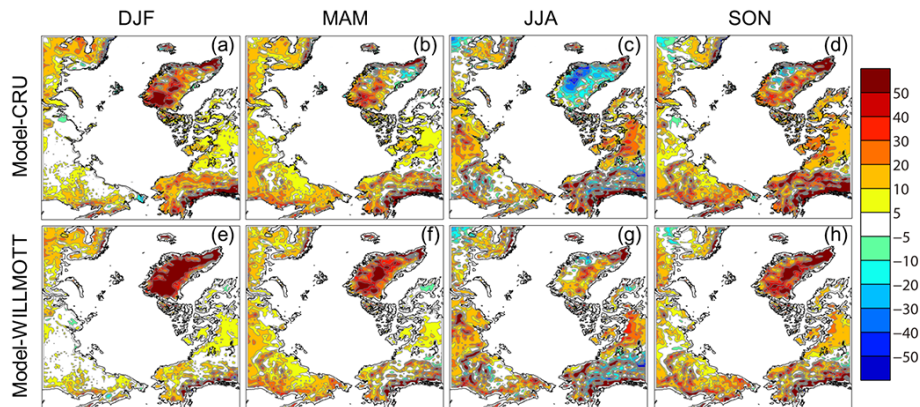


**Figure 3.** The total seasonal precipitation anomalies (mm) relative to the CRU and WILLMOTT data sets for the period 1961–1990. (a, e) Winter, December to February (DJF). (b, f) Spring, March to May (MAM). (c, g) Summer, June to August (JJA). (d, h) Autumn, September to November (SON).

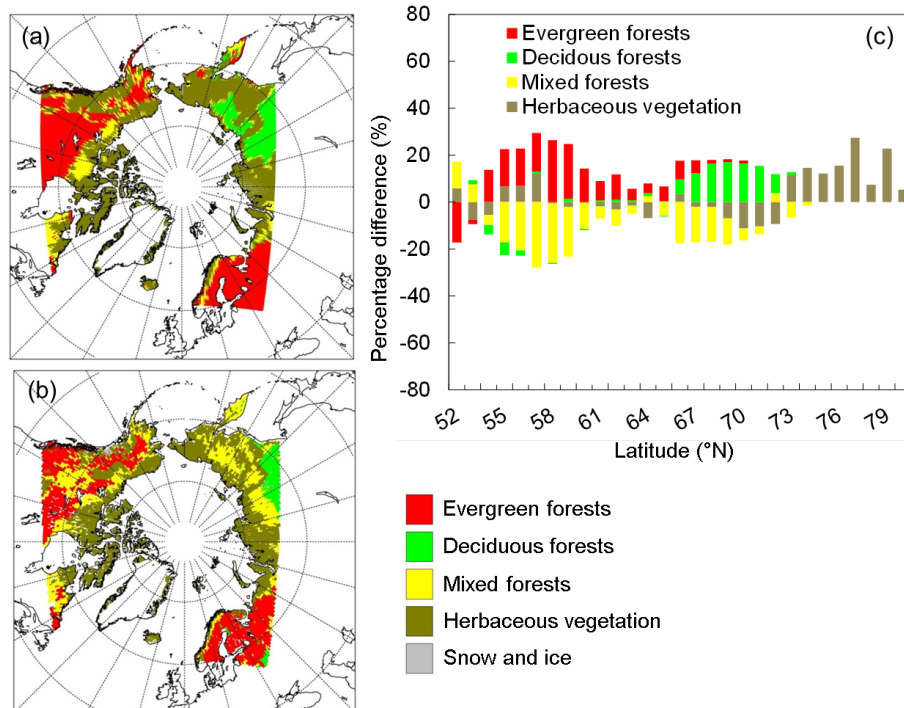


**Figure 4.** The dominant potential natural vegetation (PNV) distribution comparison for the recent period. (a) The tile-weighted PNV simulated by RCA-GUESS for the period 1961–1990. (b) The validation map derived from the ISLSCP II Potential Natural Vegetation Cover data set (Ramankutty and Foley, 2010) and the Kaplan PNV map (Kaplan et al., 2003). (c) Percentage difference (simulated minus validation map) between the number of grid cells each aggregated vegetation class occupies in each latitude band, from 52–80° N.

in both spring and summer across the entire domain except northern Canada (Fig. 2b, c, f and g). A warm bias on the order of 2 °C occurs over winter in Scandinavia, in autumn in eastern Siberia and for all seasons in northern Canada (Fig. 2a, d, e and h). The most pronounced bias in seasonal temperature is found in eastern Siberia. Greenland is an exception because both the CRU and WILLMOTT data sets are expected to have a significant bias due to poor coverage

of measurement sites. The simulated total seasonal precipitation is 5–20 mm higher compared to the validation data sets, with a relatively larger overestimation across the entire domain in spring and autumn (Fig. 3).

The vegetation simulated by RCA-GUESS agrees reasonably well with the validation map in terms of spatial distribution and the latitudinal percent difference of grid cells that each aggregated vegetation class occupies. The belt pattern

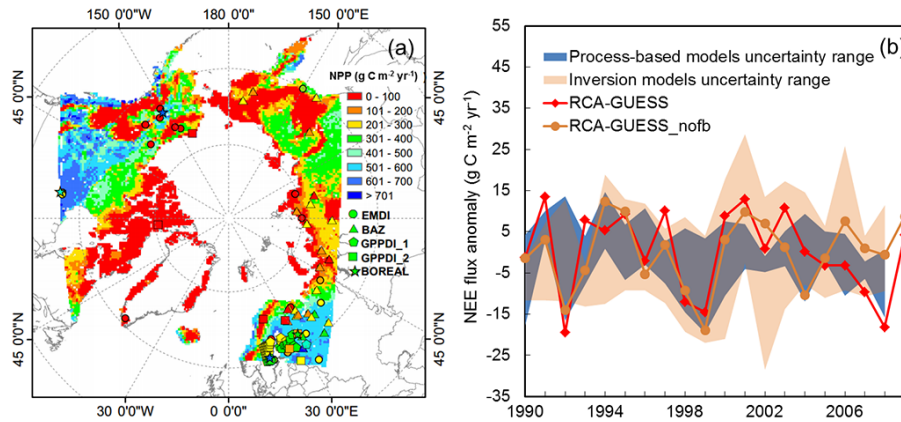


**Figure 5.** (a) The spatial distribution of the simulated mean NPP flux for the period 1961–1990 and the NPP flux validation data sets; EMDI (Olson et al., 2013a), BAZ (Denissenko et al., 2013), GPPDI\_1 (Olson et al., 2013b), GPPDI\_2 (Zheng et al., 2013), BOREAL (Gower et al., 2012). (b) The inter-annual variation of Arctic tundra NEE anomalies from the RCA-GUESS feedback and non-feedback runs, the uncertainty ranges of process-based models (LPJ-GUESS WHyMe, TEM6, TCF, Orchidee) and inversion models for the period 1990–2009.

of herbaceous vegetation across mountain ranges in Scandinavia and eastern Siberia is well displayed in both the model-derived map and the validation map (Fig. 4a and b). The latitudinal percent difference by vegetation class is generally lower than 20% (Fig. 4c). The overestimation of deciduous or evergreen forest fractions is offset by the underestimation of the mixed forests fraction. This inconsistency is partly attributed to different definitions of mixed forests in the model and validation map. In the model output, mixed forests is specified in grid cells with herbaceous fraction < 50%, and where neither evergreen nor deciduous trees cover fraction is dominant (< 33.3%). However, the validated mixed forests are classed as lands dominated by trees with a percent canopy cover > 60% and height exceeding 2 metres, consisting of tree communities with interspersed mixtures or mosaics of deciduous and evergreen types, but none of which exceeds 60% of the landscape (Loveland et al., 2000). Deciduous forests are overestimated for the herbaceous lands at the latitudes 69–73° N, as a result of a simulated tree-line situated further north in northern Canada and eastern Siberia.

The simulated mean annual NPP for 1961–1990 across Arctic tundra areas (Russian Far East Siberia, Alaska, northern Canada, eastern Siberia) is comparable to the validation data sets, and seldom exceeds  $200 \text{ g C m}^{-2} \text{ yr}^{-1}$  (Fig. 5a). Averaged over Arctic tundra, the simulated NPP for 1990–2006 is 266 or  $268 \text{ g C m}^{-2} \text{ yr}^{-1}$  (Table 1), which is broadly in line with previous estimates ( $243\text{--}252 \text{ g C m}^{-2} \text{ yr}^{-1}$  for 1960s) by the LPJ-DGVM model reported by Sitch et al. (2007). For European forest, simulated NPP exceeds observations by some  $200\text{--}300 \text{ g C m}^{-2} \text{ yr}^{-1}$  (Fig. S2 in the Supplement). This deviation indicates that nitrogen limitation and land use change are also important for predicting European forest NPP, although they were not included in this study. Similar European forest NPP estimations of approximately  $500\text{--}600 \text{ g C m}^{-2} \text{ yr}^{-1}$  are seen in simulation re-

sults with neither nitrogen limitation nor land use change from both coupled RCA-GUESS runs driven by lateral forcing fields from the reanalysis data set ERA-40 (Smith et al., 2011), and from LPJ-GUESS stand-alone simulations driven with CRU climate (Wolf et al., 2008). The simulated inter-annual variation of NEE anomalies for 1990–2006 from both RCA-GUESS runs fall within the uncertainty ranges of both process-based models and inversion models for Arctic tundra (Fig. 5b). The RCA-GUESS feedback run shows a downward trend similar to the estimates of process-based models (LPJ-GUESS WHyMe, ORCHIDEE, TCF), indicating a slight trend towards increased carbon uptake (Table 1; Fig. S3 in the Supplement). In the non-feedback run, the trend is positive, similar to results from TEM and the ensemble mean of inversions estimates. Overall, the mean annual NPP flux exceeds the sum of respiration and wildfire C emissions, resulting in a net sink of C (negative NEE) into the biosphere. Biogeophysical feedbacks have a marginal impact on this net sink, reducing it by some 5% (Table 1).

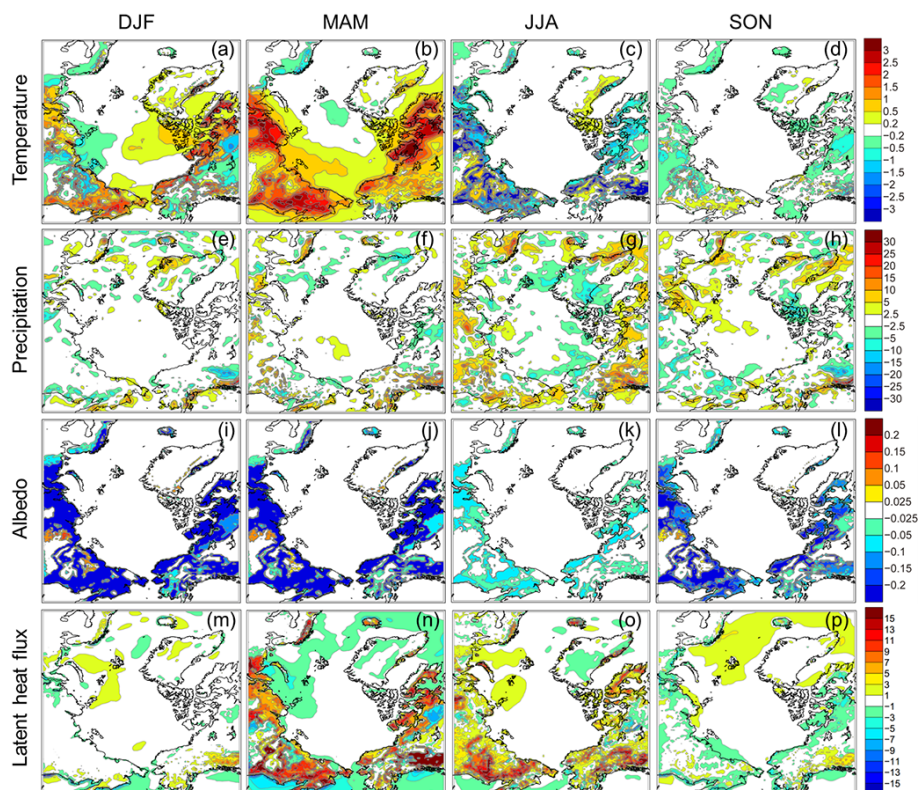
### 3.2 Impacts of biogeophysical feedbacks on Arctic climate

The influence of biogeophysical feedbacks on the simulated mean climate for 2071–2100 varies seasonally (Fig. 6a–d). The albedo feedback dominates and causes an enhanced warming in winter and spring, with the greatest additional warming of  $1.35^\circ\text{C}$  occurring in spring (Fig. 7a). The evapotranspiration feedback starts to offset the albedo feedback in spring, and reduces the warming by  $0.81^\circ\text{C}$  in summer over the Arctic as a whole, but with only a moderate influence in autumn (Figs. 6a–d and 7a). The most pronounced amplification of warming ( $\sim 3^\circ\text{C}$ ) occurs in spring across tundra areas of Siberia and northern Canada. In Fennoscandia, only the Scandes mountain range is influenced, with some additional

**Table 1.** Mean carbon budget of Arctic tundra simulated by process-based models, inversion models and RCA-GUESS for the period 1990–2006.

| Model                                 | C flux ( $\text{g C m}^{-2} \text{ yr}^{-1}$ ) |     |     |      |     | The slope of the linear trend (–) |
|---------------------------------------|--|-----|-----|------|-----|-----------------------------------|
|                                       | NPP  | RH  | NEP | FIRE | NEE |                                   |
| LPJ-GUESS WhyMe                       | –130   | 106 | –24 | 1    | –23 | –0.53                             |
| ORCHIDEE                              | –361   | 330 | –31 | –    | –31 | –0.63                             |
| TEM6                                  | –107   | 97  | –10 | 8    | –2  | 0.25                              |
| TCF                                   | –181   | 183 | –2  | –    | –2  | –0.62                             |
| The ensemble mean of inversion models | –  | –   | –   | –    | –13 | 0.2                               |
| RCA-GUESS                             | –266   | 233 | –33 | 15   | –18 | –0.35                             |
| RCA-GUESS nf.*                        | –268   | 234 | –34 | 15   | –19 | 0.24                              |

\*nf.: the non-feedback run.

**Figure 6.** The effects of biogeophysical feedbacks on 2 m temperature ( $^{\circ}\text{C}$ ) and total precipitation (mm), albedo (–) and latent heat flux ( $\text{W m}^{-2}$ ) on a seasonal basis, averaged from 2071–2100. (a, e, i, m) Winter, December to February (DJF). (b, f, j, n) Spring, March to May (MAM). (c, g, k, o) Summer, June to August (JJA). (d, h, l, p) Autumn, September to November (SON).

warming in winter and cooling in summer, which is in accordance with results reported by Wramneby et al. (2010). The impacts of biogeophysical feedbacks on precipitation are not as noticeable as for temperature. The greatest change in precipitation occurs in summer with an increase of 3.57 mm over land areas (Figs. 6e–h and 7b). In contrast to the slight albedo decline of around 0.05 in summer, albedo in autumn, winter and spring is reduced significantly across the whole tundra area with the greatest reduction of around 0.2 occurring in

spring (Fig. 6i–l). Sporadic increases of albedo are found in the larch forest belt of central Siberia from autumn to spring. An increase in latent heat flux is seen in spring and summer for most land areas except for northern Canada and eastern Siberia, where there is a reduction in magnitude (Fig. 6m–p). The largest latent heat flux increase, 9–15  $\text{W m}^{-2}$ , is seen mostly in spring, with smaller increases, 1–9  $\text{W m}^{-2}$ , in the summer months.



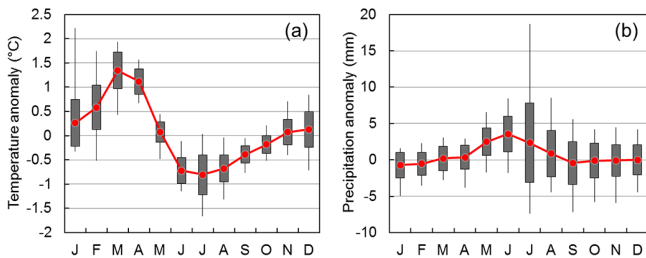


**Figure 7.** The seasonal cycle of (a) temperature anomalies ( $^{\circ}\text{C}$ ) and (b) precipitation anomalies (mm) arising from biogeophysical feedbacks for the period 2071–2100. Each box plot shows the mean (red line), one SD range (black shading) and maximum and minimum values (whiskers) for monthly climate variables.

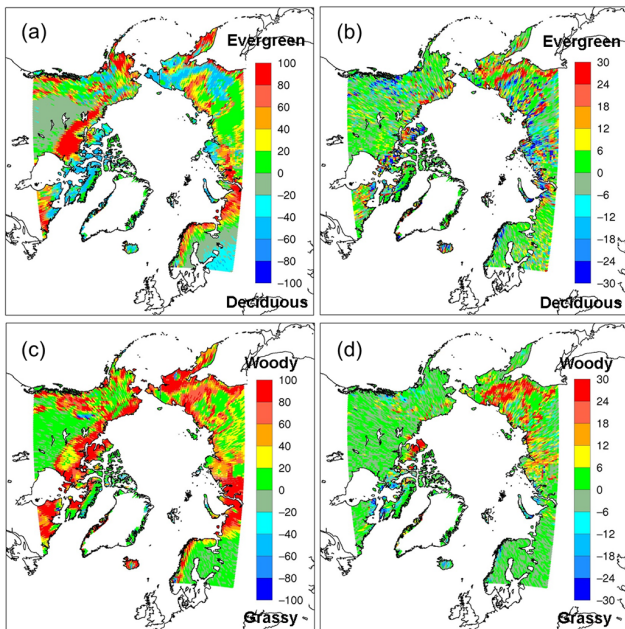


**Figure 8.** The percentage of change for normalized phenology index (%)  $C_{NPI} = (\text{LAI}_{\text{eg}} - \text{LAI}_{\text{d}}) / (\text{LAI}_{\text{eg}} + \text{LAI}_{\text{d}})$  (Wramneby et al., 2010) quantified by the shift in the relative abundance between evergreen (eg) and deciduous (d) PFTs due to (a) climate change from the period 1961–1990 to the period 2071–2100; (b) the effects of biogeophysical feedbacks for the period 2071–2100. The percentage of change for normalized physiognomy index (%)  $C_{NPMI} = (\text{LAI}_{\text{w}} - \text{LAI}_{\text{h}}) / (\text{LAI}_{\text{w}} + \text{LAI}_{\text{h}})$  quantified by the shift in the relative abundance between woody (w) and herbaceous (h) PFTs due to (c) climate change from the period 1961–1990 to the period 2071–2100; (d) the effects of biogeophysical feedbacks for the period 2071–2100.

### 3.3 Impacts of biogeophysical feedbacks on future Arctic vegetation patterns and C budget

The phenological response to the simulated climate change effects on vegetation composition is not consistent across the entire CORDEX-Arctic domain. The Scandes Mountain range, northwestern Siberia, eastern Siberia coast and

northern Canada show a substantial increase in the relative abundance of evergreen PFTs, but northeastern Europe, the Taymyr Peninsula, Russian Far East Siberia and the high Canada Arctic show an increased abundance of deciduous PFTs (Fig. 8a). Biogeophysical feedbacks tend to counteract these changes in Russian Far East Siberia, but to reinforce them in the Taymyr Peninsula (Fig. 8b). The poleward transitions from grassy PFTs to woody PFTs indicate that the tree-line boundary moves further north as a result of future climate favourable to the growth of trees (Fig. 8c). Biogeophysical feedbacks further aid the advance of woody plants into Arctic tundra in both Russian Far East Siberia and western Siberia (Fig. 8d). Compared to climate-induced shifts in vegetation abundance, the effects of biogeophysical feedbacks on vegetation distribution are relatively smaller, typically less than 30% in terms of changes to the normalized phenology and physiognomy indices (Fig. 8b, d).

The inter-annual variation of the NEE flux for 1991–2100 in the RCA-GUESS non-feedback run indicates that the C-uptake rate could start to increase rapidly in the 2020s, reach the largest value in the 2060s, after which the C-uptake rate decreases until the 2090s (Fig. 9a). However, in the RCA-GUESS feedback run, the biogeophysical feedbacks further enhance C-uptake from the 2020s, and postpone the arrival of the largest C-uptake rate for 15 years. To examine where and how many grid cells might exhibit this behaviour, we sorted the grid cells into groups according to the extent of the increase or decrease of the NEE seen in each cell. Most grid cells with the enhanced C-uptake are found in Arctic tundra with an increase of NEE around  $50\text{--}100\text{ g C m}^{-2}\text{ yr}^{-1}$ , while boreal forests show more grid cells with the largest NEE flux decreased by  $0\text{--}50\text{ g C m}^{-2}\text{ yr}^{-1}$  (Fig. 9b). Meanwhile, Arctic tundra also includes more grid cells with the largest C-uptake rate postponed than boreal forests (Fig. 9c). In total, by the end of 2100, the CORDEX-Arctic domain will gain  $38.7\text{ Gt C}$  (Table 2), of which  $35.6\text{ Gt C}$  is sequestered by Arctic tundra. This estimation is comparable to the estimates of C4MIP simulations of around  $38 \pm 20\text{ Gt C}$  for the NHLs (Qian et al., 2012). Most of the C gains are allocated to vegetation biomass. Litter and soil C stores are increased by 0.5 and 1.2 Gt C respectively for Arctic tundra, but decreased by 1.8 and 6.4 Gt C respectively for the CORDEX-Arctic domain. Biogeophysical feedbacks account for about 22% of the increase in net C uptake, around  $8.5\text{ Gt C}$ . The majority (83.5%) of this extra C uptake comes from areas simulated as Arctic tundra in the modern climate.

## 4 Discussion

### 4.1 The robustness of regional climate simulations

The biases within the down-scaled climate in an RCM may be inherited either from the systematic bias of lateral boundary conditions provided by large scale fields of climate

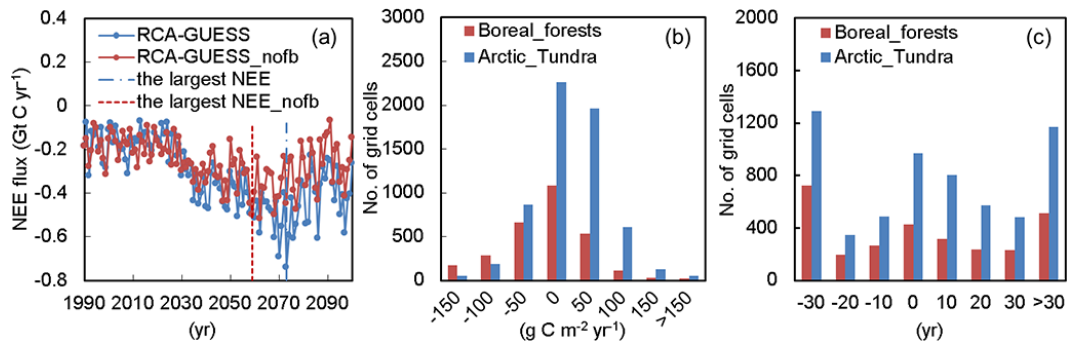


**Figure 9.** (a) The inter-annual variation of NEE flux ( $\text{Gt C yr}^{-1}$ ) in both RCA-GUESS feedback and non-feedback runs from 1990 to 2100 for Arctic tundra. (nofb: the non-feedback run; negative value: carbon sink; the vertical dash and dash-dot lines denote the year with the largest NEE over the whole period). (b) Distribution of the number of grid cells (total: 9032) for the shift of the peak C-uptake rate ( $\text{g C m}^{-2} \text{yr}^{-1}$ ) in both boreal forests and Arctic tundra (positive: increase; negative: decrease). (c) Distribution of the number of grid cells for the shift of the year (yr) with the peak C-uptake rate in both boreal forests and Arctic tundra (positive: delay; negative: advance).

**Table 2.** Carbon budget of the Arctic tundra and CORDEX-Arctic domains simulated by RCA-GUESS for the period 1990–2100.

| Domains                          | Accumulative C flux ( $\text{Gt C}$ ) |       |       |      |       | C stores ( $\text{Gt C}$ ) |       |       |
|----------------------------------|---------------------------------------|-------|-------|------|-------|----------------------------|-------|-------|
|                                  | NPP                                   | RH    | NEP   | FIRE | NEE   | VegC                       | LittC | SoilC |
| Arctic tundra fb. <sup>1</sup>   | −302.1                                | 257.7 | −44.4 | 8.8  | −35.6 | 33.9                       | 0.5   | 1.2   |
| Arctic tundra nf. <sup>2</sup>   | −288.9                                | 251.8 | −37.1 | 8.6  | −28.5 | 29.6                       | −1.3  | 0.2   |
| Arctic tundra diff. <sup>3</sup> | −13.2                                 | 5.9   | −7.3  | 0.2  | −7.1  | 4.3                        | 1.8   | 1     |
| CORDEX-Arctic fb.                | −541.2                                | 474.5 | −66.7 | 28   | −38.7 | 46.9                       | −1.8  | −6.4  |
| CORDEX-Arctic nf.                | −525.3                                | 467.1 | −58.2 | 28   | −30.2 | 42.1                       | −4    | −7.9  |
| CORDEX-Arctic diff.              | −15.9                                 | 7.4   | −8.5  | 0    | −8.5  | 4.8                        | 2.2   | 1.5   |

<sup>1</sup> fb.: the feedback run; <sup>2</sup> nf.: the non-feedback run; <sup>3</sup> diff.: the feedback run minus the non-feedback run. Note: negative values in C flux mean C uptake, but negative values in C stores mean absolute reductions of C stores.

forcing or shortcomings in the model's structures, formulations and parameterizations. For example, the warm bias over northern Canada in our simulations year-round during the period 1961–1990 is inherited from the GCM-simulated fields on the lateral boundaries of the simulated domain; the EC-Earth output shows a warm bias over this area of 1–4 °C for the 1980s, when compared to reanalysis data (Koenigk et al., 2013). For other areas of the Arctic, EC-Earth tends to show a cold bias, attributed to the overestimation of sea ice thickness and extent (Koenigk et al., 2013). This likely explains the cold bias in spring and summer found in our simulations across almost the entire domain. Berg et al. (2013) compared ERA-Interim reanalysis climate data to output from an RCA4 simulation across the Arctic forced by ERA-Interim data on the lateral boundaries, identifying a winter-time warm bias in eastern Siberia and a summer-time cold bias across the entire domain. Our simulations show similar patterns.

When similar patterns of bias recur in simulations using different lateral forcings, this may indicate the effects of inaccurate parameterizations in the model. Samuelsson et al. (2011) pointed out that RCA4 generally underestimates snow albedo in cold climate regions, resulting in higher air temperatures and less snow accumulation. This probably ex-

plains the most pronounced areas of warm bias which occur in eastern Siberia in our simulations.

Whereas the bias pattern for temperature is relatively similar between RCA-GUESS and EC-Earth, precipitation bias indicates more inconsistency. For instance, RCA-GUESS simulates less precipitation in the basins of Barents Sea and Bering Strait compared to EC-Earth. This may reflect the greater topographical variability arising from a finer grid resolution in the regional model; in EC-Earth, smoother topography reduces orographic rainfall, potentially spreading the same total amount of precipitation over a larger area, causing overestimation over rain-shadow areas in the lee of the mountain ranges. By contrast, RCA4 is known to overestimate precipitation over mountain tops due to an overestimated cloud fraction (Samuelsson et al., 2011). In general, complex mountainous terrain poses a challenge for accurately simulating vertical velocities in the resolved scale. Overall, in comparison to the EC-Earth outputs and observation-based data sets, RCA-GUESS generally demonstrates good skill in reproducing spatial patterns of the present day climate with respect to temperature and precipitation.

To verify that our climate simulation set-up, including boundary conditions from EC-Earth and the dynamic

down-scaling by the atmospheric component of RCA-GUESS, was leading to representative behaviour in the biogeochemical part of the model, we compare our simulated results for NEE, averaged across the Arctic, with the estimates from stand-alone simulations of LPJ-GUESS forced by a wide range of GCMs under the same (RCP8.5) radiative forcing scenario. Figure S4 in the Supplement compares the results from this study with results obtained by Ahlström et al. (2012b) in simulations with LPJ-GUESS forced by 18 GCMs from the CMIP5 initiative. The inter-annual variations of the cumulative NEE flux simulated in both the feedback and non-feedback runs agree well with the ensemble mean of the stand-alone simulations from 1990 to 2020. From 2020–2100, the C uptake started to increase more rapidly, but remained within the ensemble range (Fig. S4 in the Supplement). This suggests that our climate forcing set-up is representative for climate projections from a wide range of GCMs in terms of predicting the NEE flux.

#### 4.2 Vegetation dynamics and ecosystem biogeochemistry in response to Arctic climate change

Distinct geographical patterns of vegetation distribution in the Arctic and NHLs are largely shaped by spatial patterns in temperature and precipitation, while other factors like soil properties, topographical barriers, land use change, and permafrost vulnerability are additional determinants (Morales et al., 2005; Koca et al., 2006; Jiang et al., 2012). Zhang et al. (2013) demonstrated that LPJ-GUESS shows a generally good performance in replicating vegetation patterns across the Arctic, in particular capturing forest–shrub–tundra transitions observed in the Canadian Arctic, northern Alaska, the Taymyr Peninsula, and the Scandes Mountain range under the present-day climate. RCA-GUESS simulates vegetation shifts in broad agreement with previous studies: the combined effects of climatic warming and elevated CO<sub>2</sub> allow the bioclimatic niche for boreal or temperate forests to move towards higher latitudes and elevations (Fig. 8c; Morales et al., 2007; Wolf et al., 2008; Zhang et al., 2013); the longer and warmer growing season favours broad-leaved deciduous (e.g. birch) forests in competition with evergreen forests dominated by species of spruce and pine, typical for the boreal zone (Fig. 8a, c; Hickler et al., 2012; Miller and Smith, 2012; Jiang et al., 2012) and warmer winters and altered precipitation patterns result in boreal deciduous (larch) trees in Siberia giving way to boreal evergreen and temperate deciduous trees (Fig. 8a; Kaplan et al., 2003; Shuman et al., 2011; Zhang et al., 2013).

Numerous modelling studies have explored how climate-, CO<sub>2</sub>- and land use-driven variations in NPP, HR and disturbance fluxes might influence the future fate of the present-day sink of atmospheric CO<sub>2</sub> within the terrestrial biosphere (e.g. Ahlström et al., 2012b; Brovkin et al., 2006; Poulter et al., 2011;). Our simulated mean NEE flux averaged from

1990–2006 for Arctic tundra in response to recent climate forcing is similar to other process-based models (Table 1 and Fig. 5b), implying that both coupled and un-coupled process-based models agree that NPP is rising faster than soil respiration in response to near-surface warming. The inter-annual variation of NEE anomalies among all the models do not deviate too much from the ensemble mean of inversion model (top-down) estimates, because they are well constrained by the relative strength of compartment fluxes. For instance, ORCHIDEE determines the high end of the uncertainty range of estimated NPP and RH, while RCA-GUESS simulates more fire disturbances resulting in a larger inter-annual variation (Table 1). RCA-GUESS and LPJ-GUESS WHyMe share the same fire process description, in which fires are determined by the amount of above-ground litter and a soil moisture threshold (Sitch et al., 2003). However, LPJ-GUESS WHyMe is forced by the observation-based, CRU climate data set and uses an extended set of Arctic-specific PFTs, which depicts the simulated tree-line boundary with more accuracy (Zhang et al., 2013). The rapid increase of C uptake from the 2020s in both RCA-GUESS runs can be attributed to substantial climate-induced vegetation shifts and a prolonged growing-season length. However, C gains eventually decline as the increased HR flux in response to continuous climate warming outpaces the increased NPP flux. Previous studies based on the stand-alone simulations with DVMS show similar effects (e.g. Cao and Woodard 1998; Cramer et al., 2001; Lucht et al., 2006; Zhang et al., 2013).

#### 4.3 Impacts of biogeophysical feedbacks for future Arctic climate and C balance

The net impacts of biogeophysical feedbacks to future climate result largely from the opposing effects of albedo- and evapotranspiration-feedback mechanisms. Firstly, the amplified warming occurring in winter and spring is associated with positive feedbacks arising from substantial reductions of albedo (Fig 6a, b, i and j). Winter- and spring-time albedo reductions indicate that the underlying snow is masked and shaded by stems and leaves of woody vegetation, which increases both in areal extent and local density, resulting in an earlier onset of the growing season and a longer snow-free season in the future. Based on a non-linear relationship between albedo and summer vegetation biomass, Euskirchen et al. (2009) predicted that the increase of regional summer heat absorption due to potential vegetation change under future climate scenarios (A2, B1 and B2) would be  $0.34 \pm 0.23 \text{ W m}^{-2} \text{ decade}^{-1}$ , which is relatively small compared to the corresponding change expected due to a shorter snow season ( $3.3 \pm 1.24 \text{ W m}^{-2} \text{ decade}^{-1}$ ). Assuming our summer albedo decline mainly reflects the contribution from vegetation change, our results are a little larger than their estimates. The decline of summer albedo by 0.05 causes  $5\text{--}10 \text{ W m}^{-2}$ , or  $0.45\text{--}0.90 \text{ W m}^{-2} \text{ decade}^{-1}$ , in the summer heat absorption for 2071–2100 relative to 1961–1990 (Fig. S5 in the

Supplement). However, it should be noted that the estimates of Euskirchen et al. (2009) are based on stand-alone, uncoupled simulations and use a lower CO<sub>2</sub> concentration scenario. After accounting for the effects of climate–vegetation interaction and stronger CO<sub>2</sub> fertilization, their estimates would be expected to increase. Secondly, attenuated warming in summer is associated with negative feedbacks arising from increased evapotranspiration that overtake positive feedbacks arising from a reduction in albedo. The evapotranspiration is enhanced by a higher overall LAI (leaf surface for evaporation) as well as a denser forest cover, which increases surface roughness, promoting a more dynamic exchange of water vapour and energy with the atmosphere. Kasurinen et al. (2014) analysed latent heat measurement data gathered at 65 boreal and arctic eddy-covariance sites and found that from tundra to forests, latent heat flux in summer increases from  $\sim 75$  to  $\sim 90 \text{ W m}^{-2}$ , which is also in line with our estimates (Fig. 6o). On an annual basis, the net effect of these feedbacks on temperature averages a modest  $0.0069 \text{ }^\circ\text{C yr}^{-1}$  over the period 1991–2100. As for their effects on the seasonal cycle of Arctic vegetation, however, the feedbacks result in an earlier, longer and more uniform vegetation period, in terms of growing-season temperatures (Fig. 7a), promoting a substantial increase in vegetation productivity. Studies with other global ESMs have reported comparable near-surface temperature increases due to vegetation-mediated feedbacks of around  $0.0028 \text{ }^\circ\text{C yr}^{-1}$  from the 1870s to the 2080s for the NHLs as a whole (Falloon et al., 2012).

Using an iterative coupling approach, Matthes et al. (2011) investigated the sensitivity of projected regional climate change to vegetation shifts imposed on the land-surface conditions in a regional climate model (HIRHAM) applied across the Arctic. They found that woody vegetation expansion under an SRES A1B emission scenario led to a change in temperature by  $3 \text{ }^\circ\text{C}$  in winter and  $-1.5 \text{ }^\circ\text{C}$  in summer. These temperature adjustments were larger than effects attributed to freezing/thawing of soil or insulation by top organic soil horizons. Similarly, we also found the largest warming to occur in winter in areas experiencing gradual dynamic shifts from tundra to forest tundra or forest tundra to forest.

The sensitivity of vegetation distribution to the effects of biogeophysical feedbacks seems relatively modest (Fig. 8b and d). The additional C sinks arising from biogeophysical feedbacks correspond, at around 8.5 Gt C, to global anthropogenic emissions for about one year under present conditions (Table 2), relatively modest compared to some estimates of the potential losses of C from thawing permafrost across the Arctic (Schuur et al., 2013). A prolonged growing season, denser forest cover and invasion of trees into tundra result in even greater enhancements to vegetation productivity, which postpones the arrival of the peak C-uptake rate for Arctic terrestrial ecosystems. In our study, dramatic changes were found in the transition from herbaceous to woody vegetation occurring in Arctic tundra (Fig. 8c). These changes

appear to primarily account for the simulated increased C storage in areas classified as Arctic tundra in the present climate.

#### 4.4 Perspectives to improve regional ESMs

Our results highlight the significance of implementing biogeophysical mechanisms of climate–vegetation interactions in regional Earth system dynamics. Not only do biogeophysical feedbacks result in a more rapid warming on an annual average basis, but they also cause adjustments in the timing and character of the growing season that affect vegetation productivity and net C balance, with further implications for climate evolution. However, we do make some simplistic assumptions in this first trial of modelling regional Earth system dynamics over the Arctic, and there are some issues that warrant further investigation in order to improve our understanding of impacts of biogeophysical feedbacks on Arctic terrestrial ecosystems and their C balance.

Biogeophysical feedback loops should be expanded to involve energy and water flux exchanged over Arctic sea surface. Swann et al. (2010) advanced a hypothesis in which a positive albedo feedback prompts the growth of vegetation, leading to an increased flux of water vapour to the atmosphere, thereby strengthening radiative forcing. After being mixed in the atmosphere, water vapour feeds back on climate not only over land but also over the sea surface, triggering a subsequent positive sea ice feedback, which in turn warms the land surface. They found radiative forcing from water vapour changes to be of a similar magnitude as the direct short-wave forcing from albedo reductions. Therefore, further modelling studies on Arctic regional Earth system dynamics ought to include the ocean component to fully address biogeophysical feedbacks.

Permafrost C feedbacks due to future climate change should be considered when terrestrial biogeochemical cycling is coupled with biogeophysical mechanisms. Enormous amounts of organic C stored in the NHL permafrost soils could become vulnerable to decomposition, and act as a positive feedback to accelerate climate warming (Koven et al., 2011; MacDougall et al., 2012). Most terrestrial C cycling models including our model do not have representations of permafrost C dynamics, and thus may neglect the contributions to future climate change from this substantial amount of C. Recent expert assessments estimate permafrost C release for the RCP 8.5 scenario to be 162–288 Pg C by 2100 (Schuur et al., 2013). Environmental change affected by biogeophysical feedbacks could either mitigate or exacerbate permafrost degradation associated with the projected warming. Changes in regional patterns of precipitation and extra warming due to albedo- and evapotranspiration-feedbacks will likely change soil water content and temperatures, affecting the absolute and relative amounts of CO<sub>2</sub> and CH<sub>4</sub> released to the atmosphere. The cooling effects of shading by shrubs in Arctic tundra may reduce summer permafrost thaw,

even though continued warming of the Arctic may offset this negative feedback in the long term (Blok et al., 2010). Other factors such as snow redistribution, snow depth changes, and changes to shrub height, cover and expansion are also important in order to quantify the net effects of climate–vegetation interactions on permafrost thermal dynamics (Lawrence and Swenson, 2011). Increased efforts are needed to have an overall understanding of the link between permafrost C and biogeophysical mechanisms.

Discrepancies between the simulated and actual vegetation distribution can be overcome by considering factors such as land use change and more detailed vegetation types. Wraneby et al. (2010) found that land use change from croplands to forests and abandoned lands would impact the strength of the albedo- and evapotranspiration-mediated feedbacks over Europe. In mountainous areas, land-use change plays an even more important role in driving tree-line dynamics than climate change (Hickler et al., 2012). For Arctic ecosystem dynamics, terrestrial ecosystem models should be tailored to better capture a variety of Arctic and Subarctic landscapes, and include tall and low shrubs, graminoid forbs, lichen and moss. In this study, using C3 grass and trees instead of forbs and shrubs typical for Arctic tundra, we may underestimate the C-uptake strength arising from shrubs' expansion despite our model's ability to capture the grass-wood transition in a manner similar to the forests-shrubs-tundra transition seen in Zhang et al. (2013). Moreover, it is important to evaluate the algorithm to derive albedo change from simulated changes in vegetation relative cover fractions and LAI. Brovkin et al. (2013) present an approach to evaluate woody vegetation cover and land-surface albedo in ESMs that can be applied to regional studies as well.

The model version adopted for this study does not include nutrient feedbacks to vegetation growth, although N cycling is included in the current offline version of LPJ-GUESS (Smith et al., 2014). Nitrogen mineralization rates in the cold soils of boreal and Arctic ecosystems are known to limit the productivity of vegetation in these areas. Simulations with N-enabled global carbon cycle models generally suggest that C sequestration under a future high CO<sub>2</sub> climate will be lower globally when N-cycle feedbacks are accounted for (Zaehle and Dalmonech, 2011). However, increasing mineralization rates in warming soils will reduce N-limitation, allowing substantial productivity increases as growing seasons become longer and warmer. In addition, trees colonising tundra areas, which are rendered accessible by a milder climate constitute a temporary, new sink for carbon until stand-carrying capacity is reached and mortality matches biomass growth. As shown for the N-enabled version of LPJ-GUESS by Wårdlin et al. (2014), these effects will counteract any tendency for N availability to inhibit an increase in C storage by high-latitude ecosystems in a warming, high-CO<sub>2</sub> climate. Baseline (1961–1990) NPPs simulated by RCA-GUESS across the Arctic are within the range of variability of observations (Fig. 5a). Although the present study does not include N lim-

itation, the simulated increase in ecosystem C storage across the Arctic may be realistic. How nutrient cycling effects may impact biogeophysical land-climate interaction remains unclear and needs further investigation.

## 5 Conclusions

Our simulations with a regional ESM suggest that in the present climate, Arctic ecosystems are acting as a weak C sink, consistent with findings from some other process-based models and inversion studies. Under an RCP 8.5 future climate scenario, an increased C-uptake rate is projected until the 2060s–2070s, after which C uptake declines as increased soil respiration and biomass burning outpaces further increases in vegetation net primary productivity. Biogeophysical effects from climate–vegetation interactions, leading to an earlier, longer growing season and milder peak temperatures in summer, enhance the initial increase in the C sink by accentuating NPP and postponing the peak C-uptake rate by some 15 years. Integrated over the 21st century, the additional C sinks arising from biogeophysical feedbacks are some 8.5 Gt C, or 22 % of the total C sink, of which 83.5 % is located in areas currently classified as Arctic tundra. The net effects of biogeophysical feedbacks to the regional climate result from two opposing feedback mechanisms, namely the albedo feedback and the evapotranspiration feedback. The former dominates in the winter and spring seasons, amplifying the near-surface warming by up to 1.35 °C in spring, while the latter dominates in summer, resulting in an evaporative cooling of up to 0.81 °C. Such feedbacks stimulate vegetation growth with an earlier onset of the growing season, leading to compositional changes in woody plants and vegetation redistribution.

**The Supplement related to this article is available online at doi:10.5194/bg-11-5503-2014-supplement.**

*Acknowledgements.* The model simulations were carried out at the National Supercomputer Centre (NSC) in Linköping, Sweden. The study is funded by the Swedish Research Council FORMAS within the project Advanced Simulation of Arctic Climate and Impact on Northern Regions (ADSIMNOR). The authors would like to thank the Rossby Centre at the Swedish Meteorological and Hydrological Institute (SMHI) for coordinating this project, and thank A. David McGuire and Anders Ahlström for providing additional data to evaluate our results. The study is a contribution to the strategic research areas Modelling the Regional and Global Earth System (MERGE) and Biodiversity and Ecosystem Services in a Changing Climate (BECC), the Lund University Centre for the study of Climate and Carbon Cycle (LUCCI) and the Nordic Centre of Excellence DEFROST.

Edited by: R. Keeling

## References

- Ahlström, A., Miller, P. A., and Smith, B.: Too early to infer a global NPP decline since 2000. *Geophys. Res. Lett.*, 39, L15403, doi:10.1029/2012GL052336, 2012a.
- Ahlström, A., Schurgers, G., Arneth, A., and Smith, B.: Robustness and uncertainty in terrestrial ecosystem carbon response to CMIP5 climate change projections, *Environ. Res. Lett.*, 7, 044008, doi:10.1088/1748-9326/7/4/044008, 2012b.
- Bathiany, S., Claussen, M., Brovkin, V., Raddatz, T., and Gayler, V.: Combined biogeophysical and biogeochemical effects of large-scale forest cover changes in the MPI earth system model, *Biogeosciences*, 7, 1383–1399, doi:10.5194/bg-7-1383-2010, 2010.
- Beck, P. S. A. and Goetz, S. J.: Satellite observations of high northern latitude vegetation productivity changes between 1982 and 2008: ecological variability and regional differences, *Environ. Res. Lett.*, 6, 045501, doi:10.1088/1748-9326/6/4/045501, 2011.
- Berg, P., Döscher, R., and Koenigk, T.: Impacts of using spectral nudging on regional climate model RCA4 simulations of the Arctic, *Geosci. Model Dev.*, 6, 849–859, doi:10.5194/gmd-6-849-2013, 2013.
- Betts, R. A.: Offset of the potential carbon sink from boreal forestation by decreases in surface albedo, *Nature*, 408, 187–190, doi:10.1038/35041545, 2000.
- Blok, D., Heijmans, M. M. P. D., Schaepman-Strub, G., Kononov, A. V., Maximov, T. C., and Berendse, F.: Shrub expansion may reduce summer permafrost thaw in Siberian tundra, *Glob. Change Biol.*, 16, 1296–1305, 2010.
- Bonan, G. B.: Forests and Climate Change: Forcings, Feedbacks, and the Climate Benefits of Forests, *Science*, 320, 1444–1449, doi:10.1126/science.1155121, 2008.
- Bonfils, C. J. W., Phillips, T. J., Lawrence, D. M., Cameron-Smith, P., Riley, W. J., and Subin, Z. M.: On the influence of shrub height and expansion on northern high latitude climate, *Environ. Res. Lett.*, 7, 015503, doi:10.1088/1748-9326/7/1/015503, 2012.
- Brovkin, V., Claussen, M., Driesschaert, E., Fichet, T., Kicklighter, D., Loutre, M. F., Matthews, H. D., Ramankutty, N., Schaeffer, M., and Sokolov, A.: Biogeophysical effects of historical land cover changes simulated by six Earth system models of intermediate complexity, *Clim. Dynam.*, 26, 587–600, doi:10.1007/s00382-005-0092-6, 2006.
- Brovkin, V., Boysen, L., Raddatz, T., Gayler, V., Loew, A., and Claussen, M.: Evaluation of vegetation cover and land-surface albedo in MPI-ESM CMIP5 simulations, *J. Adv. Model. Earth Syst.*, 5, 48–57, doi:10.1029/2012MS000169, 2013.
- Cao, M. and Woodward, F. I.: Net primary and ecosystem production and carbon stocks of terrestrial ecosystems and their responses to climate change, *Glob. Change Biol.*, 4, 185–198, doi:10.1046/j.1365-2486.1998.00125.x, 1998.
- Chapin, F. S., Sturm, M., Serreze, M. C., McFadden, J. P., Key, J. R., Lloyd, A. H., McGuire, A. D., Rupp, T. S., Lynch, A. H., Schimel, J. P., Beringer, J., Chapman, W. L., Epstein, H. E., Euskirchen, E. S., Hinzman, L. D., Jia, G., Ping, C.-L., Tape, K. D., Thompson, C. D. C., Walker, D. A., and Welker, J. M.: Role of Land-Surface Changes in Arctic Summer Warming, *Science*, 310, 657–660, doi:10.1126/science.1117368, 2005.
- Cox, P. M., Betts, R. A., Jones, C. D., Spall, S. A., and Totterdell, I. J.: Acceleration of global warming due to carbon-cycle feedbacks in a coupled climate model, *Nature*, 408, 184–187, doi:10.1038/35041539, 2000.
- Cramer, W., Kicklighter, D. W., Bondeau, A., Moore III, B., Churkina, G., Nemry, B., Ruimy, A. and Schloss, A. L.: Comparing global models of terrestrial net primary productivity (NPP): overview and key results, *Glob. Change Biol.*, 5, 1–15, doi:10.1046/j.1365-2486.1999.00009.x, 1999.
- Denissenko, E. A., Brovkin, V., and Cramer, W.: NPP Multi-Biome: PIK Data for Northern Eurasia, 1940–1988 (Based on Bazilevich), Data set, available at: <http://daac.ornl.gov>, from Oak Ridge National Laboratory Distributed Active Archive Center, Oak Ridge, Tennessee, USA, doi:10.3334/ORNLDAAAC/575, 2013.
- Elmendorf, S. C., Henry, G. H. R., Hollister, R. D., Bjork, R. G., Boulanger-Lapointe, N., Cooper, E. J., Cornelissen, J. H. C., Day, T. A., Dorrepaal, E., Elumeeva, T. G., Gill, M., Gould, W. A., Harte, J., Hik, D. S., Hofgaard, A., Johnson, D. R., Johnstone, J. F., Jonsdottir, I. S., Jorgenson, J. C., Klanderud, K., Klein, J. A., Koh, S., Kudo, G., Lara, M., Levesque, E., Magnusson, B., May, J. L., Mercado-Diaz, J. A., Michelsen, A., Molau, U., Myers-Smith, I. H., Oberbauer, S. F., Onipchenko, V. G., Rixen, C., Martin Schmidt, N., Shaver, G. R., Spasojevic, M. J., orhallsdottir, o. E., Tolvanen, A., Troxler, T., Tweedie, C. E., Villareal, S., Wahren, C.-H., Walker, X., Webber, P. J., Welker, J. M., and Wipf, S.: Plot-scale evidence of tundra vegetation change and links to recent summer warming, *Nat. Clim. Change*, 2, 453–457, doi:10.1038/nclimate1465, 2012.
- Euskirchen, E. S., McGuire, A. D., Rupp, T. S., Chapin III, F. S., and Walsh J. E.: Projected changes in atmospheric heating due to changes in fire disturbance and the snow season in the western Arctic, 2003–2100, *J. Geophys. Res.*, 114, G04022, doi:10.1029/2009JG001095, 2009.
- Falloon, P. D., Dankers, R., Betts, R. A., Jones, C. D., Booth, B. B., and Lambert, F. H.: Role of vegetation change in future climate under the A1B scenario and a climate stabilisation scenario, using the HadCM3C Earth system model, *Biogeosciences*, 9, 4739–4756, doi:10.5194/bg-9-4739-2012, 2012.
- Gerten, D., Schaphoff, S., Haberlandt, U., Lucht, W., Sitch, S.: Terrestrial vegetation and water balance – hydrological evaluation of a dynamic global vegetation model, *J. Hydrol.*, 286, 249–270, doi:10.1016/j.jhydrol.2003.09.029, 2004.
- Gower, S.T., Krankina, O., Olson, R. J., Apps, M., Linder, S., and Wang, C.: NPP Boreal Forest: Consistent Worldwide Site Estimates, 1965–1995, R1. Data set, available at: <http://daac.ornl.gov> from the Oak Ridge National Laboratory Distributed Active Archive Center, Oak Ridge, Tennessee, USA, doi:10.3334/ORNLDAAAC/61, 2012.
- Hayes, D. J., McGuire, A. D., Kicklighter, D. W., Gurney, K. R., Burnside, T. J., and Melillo, J. M.: Is the northern high-latitude land-based CO<sub>2</sub> sink weakening? *Global Biogeochem. Cy.*, 25, GB3018, doi:10.1029/2010GB003813, 2011.
- Hayes, D. J., Turner, D. P., Stinson, G., McGuire, A. D., Wei, Y., West, T. O., Heath, L. S., de Jong, B., McConkey, B. G., Birdsey, R. A., Kurz, W. A., Jacobson, A. R., Huntzinger, D. N., Pan, Y., Post, W. M., and Cook, R. B.: Reconciling estimates of the contemporary North American carbon balance among terrestrial biosphere models, atmospheric inversions, and a new approach for estimating net ecosystem exchange from inventory-based data, *Global Change Biol.*, 18, 1282–1299, 2012.
- Hazelegger, W., Severijns, C., Semmler, T., Ștefănescu, S., Yang, S., Wang, X., Wyser, K., Dutra, E., Baldasano, J. M., Bintanja, R., Bougeault, P., Caballero, R., Ekman, A. M. L., Christensen, J. H.,

- van den Hurk, B., Jimenez, P., Jones, C., Källberg, P., Koenigk, T., McGrath, R., Miranda, P., van Noije, T., Palmer, T., Parodi, J. A., Schmith, T., Selten, F., Storelvmo, T., Sterl, A., Tapamo, H., Vancoppenolle, M., Viterbo, P., and Willén, U.: EC-Earth: a seamless earth-system prediction approach in action, *Bull. Amer. Meteor. Soc.*, 91, 1357–1363, doi:10.1175/2010BAMS2877.1, 2010.
- Hazelegger, W., Wang, X., Severijns, C., Ștefănescu, S., Bintanja, R., Sterl, A., Wyser, K., Semmler, T., Yang, S., van den Hurk, B., van Noije, T., van der Linden, E., van der Wiel, K.: EC-Earth V2.2: description and validation of a new seamless Earth system prediction model, *Clim. Dyn.*, 39, 2611–2629, 2012.
- Hickler, T., Vohland, K., Feehan, J., Miller, P. A., Smith, B., Costa, L., Giesecke, T., Fronzek, S., Carter, T. R., Cramer, W., Kühn, I., and Sykes, M. T.: Projecting the future distribution of European potential natural vegetation zones with a generalized, tree species-based dynamic vegetation model, *Global Ecol. Biogeogr.*, 21, 50–63, doi:10.1111/j.1466-8238.2010.00613.x, 2012.
- Jiang, Y., Zhuang, Q., Schaphoff, S., Sitch, S., Sokolov, A., Kicklighter, D., and Melillo, J.: Uncertainty analysis of vegetation distribution in the northern high latitudes during the 21st century with a dynamic vegetation model, *Ecology and Evolution*, 2, 593–614, doi:10.1002/ece3.85, 2012.
- Kaplan, J. O., Bigelow, N. H., Prentice, I. C., Harrison, S. P., Bartlein, P. J., Christensen, T. R., Cramer, W., Matveyeva, N. V., McGuire, A. D., Murray, D. F., Razzhivin, V. Y., Smith, B., Walker, D. A., Anderson, P. M., Andreev, A. A., Brubaker, L. B., Edwards, M. E., and Lozhkin, A. V.: Climate change and Arctic ecosystems II: Modeling, paleodata-model comparisons and future projections, *J. Geophys. Res.*, 108, 8171, doi:10.1029/2002JD002559, 2003.
- Kasurinen, V., Alfredsen, K., Kolari, P., Mammarella, I., Alekseychik, P., Rinne, J., Vesala, T., Bernier, P., Boike, J., Langer, M., Belelli Marchesini, L., van Huissteden, K., Dolman, H., Sachs, T., Ohta, T., Varlagin, A., Rocha, A., Arain, A., Oechel, W., Lund, M., Grelle, A., Lindroth, A., Black, A., Aurela, M., Laurila, T., Lohila, A., and Berninger, F.: Latent heat exchange in the boreal and arctic biomes, *Glob. Change Biol.*, doi:10.1111/gcb.12640, online first, 2014.
- Keuper, F., Parmentier, F. J., Blok, D., Bodegom, P., Dorrepaal, E., Hal, J., Logtestijn, R. P., and Aerts, R.: Tundra in the rain: differential vegetation responses to three years of experimentally doubled summer precipitation in siberian shrub and swedish bog tundra, *Ambio*, 41, 269–280, doi:10.1007/s13280-012-0305-2, 2012.
- Kimball, J. S., Jones, L. A., Zhang, K., Heinsch, F. A., McDonald, K. C., and Oechel, W. C.: A satellite approach to estimate land-atmosphere CO<sub>2</sub> exchange for Boreal and Arctic biomes using MODIS and AMSR-E, *IEEE T. Geosci. Remote*, 47, 569–587, doi:10.1109/TGRS.2008.2003248, 2009.
- Koenigk, T., Brodeau, L., Graversen, R., Karlsson, J., Svensson, G., Tjernström, M., Willén, U., and Wyser, K.: Arctic climate change in 21st century CMIP5 simulations with EC-Earth, *Clim. Dynam.*, 40, 2719–2743, doi:10.1007/s00382-012-1505-y, 2013.
- Koca, D., Smith, B., and Sykes M. T.: Modelling Regional Climate Change Effects On Potential Natural Ecosystems in Sweden, *Climatic Change*, 78, 381–406, doi:10.1007/s10584-005-9030-1, 2006.
- Koven, C. D., Friedlingstein, P., Ciais, P., Khvorostyanov, D., Krinner, G., and Tarnocai, C.: On the formation of high-latitude soil carbon stocks: Effects of cryoturbation and insulation by organic matter in a land surface model, *Geophys. Res. Lett.*, 36, L21501, doi:10.1029/2009GL040150, 2009.
- Koven, C. D., Ringeval, B., Friedlingstein, P., Ciais, P., Cadule, P., Khvorostyanov, D., Krinner, G., and Tarnocai, C.: Permafrost carbon-climate feedbacks accelerate global warming, *P. Natl. Acad. Sci.*, 108, 14769–14774, 2011.
- Kueppers, L. M., Snyder, M. A., Sloan L. C., Zavaleta, E. S., and Fulfrost, B.: Modelled regional climate change and California endemic oak ranges, *P. Natl. Acad. Sci.*, 102, 16281–16286, 2005.
- Lawrence, D. M. and Swenson S. C.: Permafrost response to increasing Arctic shrub abundance depends on the relative influence of shrubs on local soil cooling versus large-scale climate warming, *Environ. Res. Lett.*, 6, 045504, doi:10.1088/1748-9326/6/4/045504, 2011.
- Lorant, M. M., Berner, L. T., Goetz, S. J., Jin, Y., and Rander-son, J. T.: Vegetation controls on northern high latitude snow-albedo feedback: observations and CMIP5 model predictions, *Glob. Change Biol.*, 20, 594–606, doi:10.1111/gcb.12391, 2014.
- Loveland, T. R., Reed B. C., Brown J. F., Ohlen D. O., Zhu Z., Yang L., and Merchant J. W.: Development of a global land cover characteristics database and IGBP DISCover from 1 km AVHRR data, *Int. J. Remote Sens.*, 21, 1303–1330, doi:10.1080/014311600210191, 2000.
- Lucht W., Schaphoff S., Erbrecht T., Heyder U., and Cramer W.: Terrestrial vegetation redistribution and carbon balance under climate change, *Carbon Balance and Management*, p. 7, 2006.
- MacDougall, A. H., Avis C. A., and Weaver A. J.: Significant contribution to climate warming from the permafrost carbon feedback, *Nat. Geosci.*, 5, 719–721, doi:10.1038/ngeo1573, 2012.
- Matthes, H., Rinke, A., Miller, P., Kuhry, P., Dethloff, K., and Wolf, A.: Sensitivity of high-resolution Arctic regional climate model projections to different implementations of land surface processes, *Climatic Change*, 111, 197–214, doi:10.1007/s10584-011-0138-1, 2011.
- McGuire, A. D., Hayes, D. J., Kicklighter, D. W., Manizza, M., Zhuang, Q., Chen, M., Follows, M. J., Gurney, K. R., McClelland, J.W., Melillo, J.M., Peterson, B. J., and Prinn, R.: An analysis of the carbon balance of the Arctic Basin from 1997 to 2006, *Tellus B*, 62, 455–474, doi:10.1111/j.1600-0889.2010.00497.x, 2010.
- McGuire, A. D., Christensen, T. R., Hayes, D., Heroult, A., Euskirchen, E., Kimball, J. S., Koven, C., Lafleur, P., Miller, P. A., Oechel, W., Peylin, P., Williams, M., and Yi, Y.: An assessment of the carbon balance of Arctic tundra: comparisons among observations, process models, and atmospheric inversions, *Biogeosciences*, 9, 3185–3204, doi:10.5194/bg-9-3185-2012, 2012.
- Miller, P. A. and Smith, B.: Modelling Tundra Vegetation Response to Recent Arctic Warming, *Ambio*, 41, 281–291, doi:10.1007/s13280-012-0306-1, 2012.
- Mitchell, T. D. and Jones, P. D.: An improved method of constructing a database of monthly climate observations and associated high-resolution grids, *Int. J. Climatol.*, 25, 693–712, doi:10.1002/joc.1181, 2005.
- Monson, R. K., Lipson, D. L., Burns, S. P., Turnipseed, A. A., Delany, A. C., Williams M. W., and Schmidt S. K.: Winter forest soil

- respiration controlled by climate and microbial community composition, *Nature*, 439, 711–714, doi:10.1038/nature04555, 2006.
- Morales, P., Sykes, M. T., Prentice, I. C., Smith, P., Smith, B., Bugmann, H., Zierl, B., Friedlingstein, P., Viovy, N., Sabaté, S., Sánchez, A., Pla, E., Gracia, C. A., Sitch, S., Arneth, A., and Ogee, J.: Comparing and evaluating process-based ecosystem model predictions of carbon and water fluxes in major European forest biomes, *Glob. Change Biol.*, 11, 2211–2233, doi:10.1111/j.1365-2486.2005.01036.x, 2005.
- Morales, P., Hickler, T., Rowell, D. P., Smith, B., and Sykes, M. T.: Changes in European ecosystem productivity and carbon balance driven by regional climate model output, *Glob. Change Biol.*, 13, 108–122, doi:10.1111/j.1365-2486.2006.01289.x, 2007.
- Moss, R. H., Edmonds, J. A., Hibbard, K. A., Manning, M. R., Rose, S. K., van Vuuren, D. P., Carter, T. R., Emori, S., Kainuma, M., Kram, T., Meehl, G. A., Mitchell, J. F. B., Nakicenovic, N., Riahi, K., Smith, S. J., Stouffer, R. J., Thomson, A. M., Weyant, J. P., and Wilbanks, T. J.: The next generation of scenarios for climate change research and assessment, *Nature*, 463, 747–756, doi:10.1038/nature08823, 2010.
- Olson, R. J., Scurlock, J. M. O., Prince, S. D., Zheng, D. L., and Johnson, K. R. (Eds.): NPP Multi-Biome: NPP and Driver Data for Ecosystem Model Data Intercomparison, R2. Data set, available at: <http://daac.ornl.gov>, from Oak Ridge National Laboratory Distributed Active Archive Center, Oak Ridge, Tennessee, USA, doi:10.3334/ORNLDAAAC/615, 2013a.
- Olson, R. J., Scurlock, J. M. O., Prince, S. D., Zheng, D. L., and Johnson, K. R. (Eds.): NPP Multi-Biome: Global Primary Production Data Initiative Products, R2. Data set, available at: <http://daac.ornl.gov>, from the Oak Ridge National Laboratory Distributed Active Archive Center, Oak Ridge, Tennessee, USA, doi:10.3334/ORNLDAAAC/617, 2013b.
- Oechel, W. C., Hastings, S. J., Vourlirts, G., Jenkins, M., Riechers, G., and Grulke, N.: Recent change of Arctic tundra ecosystems from a net carbon dioxide sink to a source, *Nature*, 361, 520–523, doi:10.1038/361520a0, 1993.
- Pan, Y., Birdsey, R. A., Fang, J., Houghton, R., Kauppi, P. E., Kurz, W. A., Phillips, O. L., Shvidenko, A., Lewis, S. L., Canadell, J. G., Ciais, P., Jackson, R. B., Pacala, S. W., McGuire, A. D., Piao, S., Rautiainen, A., Sitch, S., and Hayes, D.: A Large and Persistent Carbon Sink in the World's Forests, *Science*, 333, 988–993, doi:10.1126/science.1201609, 2011.
- Peylin, P., Law, R. M., Gurney, K. R., Chevallier, F., Jacobson, A. R., Maki, T., Niwa, Y., Patra, P. K., Peters, W., Rayner, P. J., Rödenbeck, C., van der Laan-Luijkx, I. T., and Zhang, X.: Global atmospheric carbon budget: results from an ensemble of atmospheric CO<sub>2</sub> inversions, *Biogeosciences*, 10, 6699–6720, doi:10.5194/bg-10-6699-2013, 2013.
- Piao, S., Fang, J., Zhou, L., Ciais, P., and Zhu, B.: Variations in satellite-derived phenology in China's temperate vegetation, *Glob. Change Biol.*, 12, 672–685, doi:10.1111/j.1365-2486.2006.01123.x, 2006.
- Piao, S., Sitch, S., Ciais, P., Friedlingstein, P., Peylin, P., Wang, X., Ahlström, A., Anav, A., Canadell, J. G., Cong, N., Huntingford, C., Jung, M., Levis, S., Levy, P. E., Li, J., Lin, X., Lomas, M. R., Lu, M., Luo, Y., Ma, Y., Myneni, R. B., Poulter, B., Sun, Z., Wang, T., Viovy, N., Zaehle, S. and Zeng, N.: Evaluation of terrestrial carbon cycle models for their response to climate variability and to CO<sub>2</sub> trends, *Glob. Change Biol.*, 19, 2117–2132, doi:10.1111/gcb.12187, 2013.
- Poulter, B., Frank, D. C., Hodson, E. L., and Zimmermann, N. E.: Impacts of land cover and climate data selection on understanding terrestrial carbon dynamics and the CO<sub>2</sub> airborne fraction, *Biogeosciences*, 8, 2027–2036, doi:10.5194/bg-8-2027-2011, 2011.
- Qian, H., Joseph, R., and Zeng, N.: Enhanced terrestrial carbon uptake in the Northern High Latitudes in the 21st century from the Coupled Carbon Cycle Climate Model Intercomparison Project model projections, *Glob. Change Biol.*, 16, 641–656, doi:10.1111/j.1365-2486.2009.01989.x, 2010.
- Quillet, A., Peng, C., and Garneau, M.: Toward dynamic global vegetation models for simulating vegetation–climate interactions and feedbacks: recent developments, limitations, and future challenges, *Environ. Rev.*, 18, 333–353, doi:10.1139/A10-016, 2010.
- Ramankutty, N. and Foley, J. A.: ISLSCP II Potential Natural Vegetation Cover, in: ISLSCP Initiative II Collection, Data set, edited by: Hall F. G., Collatz, G., Meeson, B., Los, S., Brown de Colstoun, E., and Landis D., Oak Ridge National Laboratory Distributed Active Archive Center, Oak Ridge, Tennessee, USA, doi:10.3334/ORNLDAAAC/961, 2010.
- Ruckstuhl, K. E., Johnson, E., and Miyanishi, K.: Introduction. The boreal forest and global change, *Philos. T. Roy. Soc. Biol. Sci.*, 363, 2245–2249, doi:10.1098/rstb.2007.2196, 2008.
- Rummukainen, M.: State-of-the-art with regional climate models, *Wiley Interdisciplinary Reviews, Climate Change*, 1, 82–96, doi:10.1002/wcc.8, 2010.
- Samuelsson, P., Gollvik, S., and Ullerstig, A.: The land-surface scheme of the Rossby Centre regional atmospheric climate model (RCA3), *Reports Meteorol. Climatol.*, 12, p. 38, 2006.
- Samuelsson, P., Jones, C. G., WillÉN, U., Ullerstig, A., Gollvik, S., Hansson, U. L. F., Jansson, C., Kjellström, E., Nikulin, G., and Wyser, K.: The Rossby Centre Regional Climate model RCA3: model description and performance, *Tellus A*, 63, 4–23, doi:10.1111/j.1600-0870.2010.00478.x, 2011.
- Seneviratne, S. I., Corti, T., Davin, E. L., Hirschi, M., Jaeger, E. B., Lehner, I., Orlowsky, B., and Teuling, A. J.: Investigating soil moisture–climate interactions in a changing climate: A review, *Earth-Sci. Rev.*, 99, 125–161, doi:10.1016/j.earscirev.2010.02.004, 2010.
- Schuur, E. A. G., Abbott, B. W., Bowden, W. B., Brovkin, V., Camill, P., Canadell, J. G., Chanton, J. P., Chapin III, F. S., Christensen, T. R., Ciais, P., Crosby, B. T., Czimczik, C. I., Grosse, G., Harden, J., Hayes, D. J., Hugelius, G., Jastrow, J. D., Jones, J. B., Kleinen, T., Koven, C. D., Krinner, G., Kuhry, P., Lawrence, D. M., McGuire, A. D., Natali, S. M., O'Donnell, J. A., Ping, C. L., Riley, W. J., Rinke, A., Romanovsky, V. E., Sannel, A. B. K., Schädel, C., Schaefer, K., Sky, J., Subin, Z. M., Tarnocai, C., Turetsky, M. R., Waldrop, M. P., Walter Anthony, K. M., Wickland, K. P., Wilson, C. J., and Zimov, S. A.: Expert assessment of vulnerability of permafrost carbon to climate change, *Climatic Change*, 119, 359–374, 2013.
- Shuman, J. K., Shugart, H. H., and O'Halloran, T. L.: Sensitivity of Siberian larch forests to climate change, *Glob. Change Biol.*, 17, 2370–2384, 2011.
- Sitch, S., Smith, B., Prentice, I. C., Arneth, A., Bondeau, A., Cramer, W., Kaplan, J. O., Levis, S., Lucht, W., Sykes, M. T., Thonicke, K., and Venevsky, S.: Evaluation of ecosystem dynam-



- ics, plant geography and terrestrial carbon cycling in the LPJ dynamic global vegetation model, *Glob. Change Biol.*, 9, 161–185, doi:10.1046/j.1365-2486.2003.00569.x, 2003.
- Sitch, S., McGuire, A. D., Kimball, J., Gedney, N., Gamon, J., Engstrom, R., Wolf, A., Zhuang, Q., Clein, J., and McDonald, K. C.: Assessing the carbon balance of circumpolar arctic tundra using remote sensing and process modeling, *Ecol. Appl.*, 17, 213–234, 2007.
- Sitch, S., Huntingford, C., Gedney, N., Levy, P. E., Lomas, M., Piao, S. L., Betts, R., Ciais, P., Cox, P., Friedlingstein, P., Jones, C. D., Prentice, I. C., and Woodward, F. I.: Evaluation of the terrestrial carbon cycle, future plant geography and climate carbon cycle feedbacks using five dynamic global vegetation models (DGVMs), *Glob. Change Biol.*, 14, doi:10.1111/j.1365-2486.2008.01626.x, 2008.
- Smith, B., Prentice, I. C., and Sykes, M. T.: Representation of vegetation dynamics in the modelling of terrestrial ecosystems: comparing two contrasting approaches within European climate space, *Global Ecol. Biogeogr.*, 10, 621–637, doi:10.1046/j.1466-822X.2001.t01-1-00256.x, 2001.
- Smith, B., Samuelsson, P., Wramneby, A., and Rummukainen, M.: A model of the coupled dynamics of climate, vegetation and terrestrial ecosystem biogeochemistry for regional applications, *Tellus A*, 63, 87–106, doi:10.1111/j.1600-0870.2010.00477.x, 2011.
- Smith, B., Wårlind, D., Arneeth, A., Hickler, T., Leadley, P., Siltberg, J., and Zaehle, S.: Implications of incorporating N cycling and N limitations on primary production in an individual-based dynamic vegetation model, *Biogeosciences*, 11, 2027–2054, doi:10.5194/bg-11-2027-2014, 2014.
- Swann, A. L., Fung, I. Y., Levis, S., Bonan, G., and Doney, S.: Changes in Arctic vegetation induce high-latitude warming through the greenhouse effect, *P. Natl. Acad. Sci. USA*, 107, 1295–1300, doi:10.1073/pnas.0913846107, 2010.
- Tape, K. E. N., Sturm, M., and Racine, C.: The evidence for shrub expansion in Northern Alaska and the Pan-Arctic, *Glob. Change Biol.*, 12, 686–702, doi:10.1111/j.1365-2486.2006.01128.x, 2006.
- Valentini, R., Matteucci, G., Dolman, A. J., Schulze, E. D., Rebmann, C., Moors, E. J., Granier, A., Gross, P., Jensen, N. O., Pilegaard, K., Lindroth, A., Grelle, A., Bernhofer, C., Grunwald, T., Aubinet, M., Ceulemans, R., Kowalski, A. S., Vesala, T., Rannik, U., Berbigier, P., Loustau, D., Gumundsson, J., Thorgeirsson, H., Ibrom, A., Morgenstern, K., Clement, R., Moncrieff, J., Montagnani, L., Minerbi, S., and Jarvis, P. G.: Respiration as the main determinant of carbon balance in European forests, *Nature*, 404, 861–865, doi:10.1038/35009084, 2000.
- Wania, R., Ross, I., and Prentice, I. C.: Integrating peatlands and permafrost into a dynamic global vegetation model: I. Evaluation and sensitivity of physical land surface processes, *Global Biogeochem. Cy.*, 23, GB3014, doi:10.1029/2008GB003412, 2009a.
- Wania, R., Ross, I., and Prentice, I. C.: Integrating peatlands and permafrost into a dynamic global vegetation model: II. Evaluation and sensitivity of vegetation and carbon cycle processes, *Global Biogeochem. Cy.*, 23, GB015, doi:10.1029/2008GB003413, 2009b.
- Wania, R., Ross, I., and Prentice, I. C.: Implementation and evaluation of a new methane model within a dynamic global vegetation model: LPJ-WHyMe v1.3.1, *Geosci. Model Dev.*, 3, 565–584, doi:10.5194/gmd-3-565-2010, 2010.
- Wårlind, D., Smith, B., Hickler, T., and Arneeth, A.: Nitrogen feedbacks increase future terrestrial ecosystem carbon uptake in an individual-based dynamic vegetation model, *Biogeosciences Discuss.*, 11, 151–185, doi:10.5194/bgd-11-151-2014, 2014.
- Willmott, C. J. and Matsuura, K.: Smart interpolation of annually averaged air temperature in the United States, *J. Appl. Met.*, 34, 2577–2586, 1995.
- Wolf, A., Callaghan, T., and Larson, K.: Future changes in vegetation and ecosystem function of the Barents Region, *Climatic Change*, 87, 51–73, doi:10.1007/s10584-007-9342-4, 2008.
- Wramneby, A., Smith, B., and Samuelsson, P.: Hot spots of vegetation-climate feedbacks under future greenhouse forcing in Europe, *J. Geophys. Res.*, 115, D21119, doi:10.1029/2010jd014307, 2010.
- Zaehle, S. and Dalmonech, D.: Carbon-nitrogen interactions on land at global scales: understanding in modelling climate biosphere feedbacks, *Curr. Opin. Environ. Sustain.*, 3, 311–320, 2011.
- Zhang, W., Miller, P. A., Smith, B., Wania, R., Koenigk, T., and Döscher, R.: Tundra shrubification and tree-line advance amplify arctic climate warming: results from an individual-based dynamic vegetation model, *Environ. Res. Lett.*, 8, 034023, doi:10.1088/1748-9326/8/3/034023, 2013.
- Zheng, D. L., Prince, S. D., and Wright, R.: NPP Multi-Biome: Gridded Estimates for Selected Regions Worldwide, 1954–1998, R3. Data set, available at: <http://daac.ornl.gov>, from the Oak Ridge National Laboratory Distributed Active Archive Center, Oak Ridge, Tennessee, USA, doi:10.3334/ORNLDAAAC/614, 2013.